Published in final edited form as:
Nanomedicine. 2012 February ; 8(2): 250–260. doi:10.1016/j.nano.2011.06.008.

Chitosan Enhances the Stability and Targeting of Immuno-Nanovehicles to Cerebro-vascular Deposits of Alzheimer's Disease Amyloid Protein

Kristen M. Jaruszewski, MS[a], **Subramanian Ramakrishnan, PhD**[b], **Joseph F. Poduslo, PhD**[c], and **Karunya K. Kandimalla, PhD**[a,c]

[a]Department of Basic Pharmaceutical Sciences, College of Pharmacy and Pharmaceutical Sciences, Florida A & M University, Tallahassee, Florida, United States of America

[b]Department of Chemical and Biomedical Engineering, College of Engineering, Florida A&M University-Florida State University, Tallahassee, Florida, United States of America

[c]Molecular Neurobiology Laboratory, Departments of Neurology, Neuroscience, and Biochemistry/Molecular Biology, Mayo Clinic College of Medicine, Rochester, Minnesota, United States of America

Abstract

Alzheimer's disease amyloid β (Aβ) proteins accumulate in the cerebral vasculature and cause cerebral amyloid angiopathy (CAA). The objective of this study is to resolve critical formulation issues in developing nanoparticles capable of permeating the blood brain barrier (BBB) and targeting cerebrovascular Aβ proteins. To achieve this objective we designed immuno-nanovehicles, which are chitosan coated poly lactic-co-glycolic acid (PLGA) nanoparticles conjugated with a novel anti-Aβ antibody. Measurements made according to Derjaguin-Landau-Verwey-Overbeek (DLVO) theory indicated that the immuno-nanovehicles have a much lower propensity to aggregate than the control nanovehicles. Immuno-nanovehicles showed enhanced uptake at the BBB and better targeting of the Aβ proteins deposited in the CAA model in vitro compared to the control nanovehicles. In addition, chitosan enhanced aqueous dispersibility and increased the stability of immuno-nanovehicles during lyophilization thus transforming them into ideal vehicles for delivering therapeutic/diagnostic agents to the cerebral vasculature ridden with vascular amyloid.

Keywords

immuno-nanovehicle; cerebrovascular delivery; colloidal stability; cerebral amyloid angiopathy; blood brain barrier

Correspondence: Karunya K. Kandimalla, Ph.D., 228 Dyson Pharmacy Building, College of Pharmacy and Pharmaceutical Sciences, Florida A&M University, Tallahassee, FL 32307, USA; Telephone: (850)-599-3581. karunya.kandimalla@famu.edu.

In addition, there are no known conflicts of interest.

1. Background

The deposition of toxic amyloid beta (Aβ) proteins in the brain vasculature results in cerebral amyloid angiopathy (CAA). Approximately 90% of Alzheimer's disease (AD) patients and 30% of individuals over 60 have cerebrovascular amyloid (CVA) deposits . Several studies have demonstrated that AD subjects with CAA show a decline in cognitive test performance during life. In addition to causing cerebrovascular inflammation, CAA triggers vascular dysfunction, which is believed to accelerate AD progression. The current study is aimed at designing an immuno-nanovehicle capable of detecting and ultimately treating CAA. The challenges of designing nanovehicles to target CVA arise from improving the uptake of nanoparticles at the blood brain barrier (BBB) and retaining them in the cerebral vasculature for a desired duration of time; recognition and binding of nanovehicles to CVA deposits; ensuring the stability of nanovehicles during lyophilization; and ascertaining aqueous dispersibility and colloidal stability of the lyophilized nanovehicles.

The uptake of nanovehicles at the BBB and their retention in the basement membrane of the cerebral vasculature can be enhanced by carefully modulating their size and surface characteristics. Attempts have been made in the past to harness active transport processes at the BBB to enhance the endocytosis of nanoparticles by conjugating a cell surface receptor ligand or antibody on the nanoparticle surface . However, this method is very expensive and the ligand-receptor specificity more often impairs endocytosis efficiency. For example, endothelial targeting and intracellular destination of polymer carriers targeted to ICAM-1 on the endothelial cells surface are affected by the size and shape the carrier (5). In addition, Rensen et al. demonstrated that particles larger than 70 nm cannot be delivered to hepatocytes via the asialoglycoprotein receptor (6). Therefore, several research groups, including us, have championed the approach of promoting endocytosis by initiating biophysical interactions of the permeant with the cell surface. We have previously demonstrated that by conjugating polyamines such as putrescine to proteins, the BBB permeability of a permeant could be enhanced (7), which is believed to be mediated by electrostatic interactions of the positively charged permeant with the negatively charged endothelial cell surface (8).

A similar approach has been followed in this study to enhance the cellular uptake of immuno-nanovehicles conjugated with a novel anti-amyloid antibody IgG4.1 raised against human fibrillar Aβ protein that can recognize and bind to Aβ rich amyloid deposits (9–11). These nanovehicles consist of a poly lactic-co-glycolic acid nanocore coated with another biocompatible and biodegradable polymer, chitosan, which enhances positive charge density on the nanoparticle surface at physiological pH. In addition to increasing cellular uptake, the positive charges on the nanovehicle surface enhance its aqueous dispersibility. Moreover, due to structural similarity with sugars that are widely used as cryoprotectants, chitosan also serves as a cryoprotectant capable of preserving the integrity of nanoparticles as well as the proteins conjugated to the nanovehicle surface during lyophilization. This study, therefore, documents the development of immuno-nanovehicles for BBB transcytosis and specific targeting to amyloid deposits accumulated in the endothelial cells. Such nanovehicles could be employed to detect and treat cerebral amyloid angiopathy.

2. Material and Methods

Methylene chloride was obtained from Fisher Scientific (Fair Lawn, NJ, USA). Bicinchoninic acid protein assay kit was obtained from Thermo Scientific (Rockford, IL, USA). Vivaspin 20 (1,000,000 MWCO) was obtained from Sartorius Stedim (Bohemia, NY, USA). Polysorbate 20 was obtained from Bio-Rad (Hercules, CA, USA). Dulbecco's

modified Eagle's medium (DMEM) and other cell growth media ingredients were obtained from Mediatech inc. (Manassas, VA, USA). Gibco fetal bovine serum was obtained from Invitrogen (Carlsbad, CA, USA). IgG4.1 is a monoclonal antibody raised against human fibrillar Aβ42 developed at the Mayo Clinic (Rochester, MN, USA) (9). All other chemicals were obtained from Sigma Chemical Co (St. Louis, MO, USA). Poly lactic-co-glycolic acid (PLGA) 50/50 (MW 153,000) was a generous gift from Purac Biomaterials.

2.1. Preparation and Characterization of Nanoparticles

a) Chitosan Coated PLGA Nanoparticles—The CPLGA nanoparticles coated with chitosan (CPLGAnp) were prepared using methods described elsewhere (12–13). The nanoparticle suspension was centrifuged at 5,000 rpm for 10 minutes to eliminate debris and larger particulates. The supernatant containing nanoparticles was lyophilized with either 1% sucrose, 1% trehalose, or no cryo-protectant.

b) Quantification of Chitosan Adsorbed to PLGA Nanoparticles—A standard curve was prepared using medium molecular weight chitosan (MW 190,000–310,000) 1–3 mg/ml and cibacron brilliant red (14–15). To quantify chitosan adsorbed on the surface of PLGA nanoparticles, a 100 μl aliquot of 15 mg/ml CPLGAnp or PLGAnp suspension was mixed with 100 μl of 300 μg/ml of cibacron red and the pH was adjusted to 3.5. The mixture was then added to a 96-well plate and the absorbance was read at 5 nm intervals ranging from 400 nm to 750nm using a SpectraMax Plus spectrophotometer (Molecular Devices, Sunnyvale, CA, USA).

c) Naked PLGA Nanoparticles (PLGAnp)—The PLGAnp were prepared using the same procedure described above, but without chitosan in the aqueous phase.

d) Chitosan Coated PLGA Nanoparticles Loaded with 6-Coumarin (6CMR-CPLGAnp)—The 6CMR-CPLGAnp were prepared using the same method as above, except 6-coumarin (1 mg/ml) was added to the oil phase.

The particle size of PLGAnp, CPLGAnp, and 6CMR-CPLGAnp, before and after lyophilization, was measured by Brookhaven instruments BI-200SM laser light scattering system (Brookhaven Instruments, Holtsville, NY, USA), whereas the zeta potential was determined using Brookhaven Zeta Plus machine (Brookhaven Instruments, Holtsville, NY, USA).

e) Optimization of Surfactant Concentration—To achieve the optimal particle size of CPLGAnp and 6CMR-CPLGAnp, various PVA concentrations were used and the corresponding changes in particle size and zeta potential were recorded.

f) Efficiency of 6CMR encapsulation—A 1,000,000 molecular weight cut off (MWCO) spin filter was used to eliminate the un-encapsulated dye. Next, the nanoparticle suspension was washed with PBS and then re-centrifuged at 3,000 rpm for 5 minutes. Finally, the fluorescence signals of the nanoparticle suspension before filtration, after filtration, and the filtrate was measured using Tecan spectrofluorometer.

$$\text{Encapsulation efficiency} = \frac{\text{Fluorescence of 6CMR in nanoparticles}}{\text{Fluorescence of 6CMR in nanoparticles} + \text{Fluorescence of free 6CMR}} \times 100 \quad (1)$$

g) The Leakage of 6CMR Loaded CPLGAnp—The 6CMR leakage from the nanoparticles was measured by evaluating the amount of fluorescence released from the

nanoparticle suspension at various time intervals. Both lyophilized and freshly prepared nanoparticles were used in these studies. The fluorescence signal of suspensions prepared from lyophilized and unlyophilized nanoparticles was kept the same. The samples were incubated under constant stirring (200 rpm) at 37 °C. An aliquot of each nanosuspension was withdrawn at various time points up to three days and the nanoparticle suspensions were replenished with equal volume of PBS. Each aliquot thus obtained was filtered using a 1,000,000 molecular weight cut off (MWCO) spin filter, previously coated with 1% BSA, at 3,000 rpm for 5 minutes. The fluorescence signal from 200 μL of the filtrate, which contains 6-CMR released from the nanocore, was assayed using Tecan spectrofluorometer.

2.2. Preparation and Characterization of Immuno-nanovehicles (CPLGA-IgG4.1np, Figure 1)

a) Conjugation of Anti-amyloid Antibody IgG4.1 to CPLGAnp or 6CMR-CPLGAnp—The IgG4.1 was covalently conjugated to the core of the immuno-nanovehicle via carbodiimide reaction. The CPLGAnp or 6CMR-CPLGAnp were re-dispersed in PBS and the pH of the suspension was adjusted to 7.0. Various concentrations of IgG4.1: 0.2 mg, 0.5 mg, and 1.0 mg were employed in the reaction to arrive at the optimal IgG4.1 concentration required for conjugation. The unconjugated IgG4.1 was removed through spin-filtration in a 1,000,000 molecular weight cut off (MWCO) spin filter previously coated with 1% BSA.

b) Determination of the Amount of IgG4.1 Present on the Immuno-nanovehicles—A 0.5 mg aliquot of immuno-nanovehicles were suspended in 2 ml distilled water and assayed using bicinchoninic acid (BSA) protein assay kit (Thermo Scientific, Rockford, IL, USA) as per the protocols recommended by the manufacturer.

c) Enzyme Linked Immunosorbent Assay (ELISA)—The immunoreactivity of IgG4.1 incorporated in various immuno-nanovehicle formulations was examined by ELISA method developed in our lab and published elsewhere (7).

2.3. Derjaguin-Landau-Verwey-Overbeek (DLVO) Theory

According to the DLVO theory (28), the total potential energy (V_T) of interaction, which determines the colloid stability, between two particles is defined as:

$$V_T = V_A + V_E \quad (2)$$

The term V_A, the energy of interaction between the particles due to van der Waals dispersion forces, is expressed as

$$V_A = \frac{A}{6}\left[\frac{2a^2}{r^2 - 4a^2} + \frac{2a^2}{r^2} + \ln\left(1 - 4\frac{a^2}{r^2}\right)\right] \quad (3)$$

where A is the Hamaker constant for particles interacting in the medium (water), a is the particle radius and r is the distance between the centres of the particles.

The quantity V_E represents the repulsive interaction between the electrical double layers of the particles. According to the constant potential model, a reasonable expression to V_E (for moderate potential in the Stern layer, < 50 mV), is:

$$V_E = \frac{4\pi\varepsilon\varepsilon_o a^2 \psi_o^2}{r} e^{-\kappa(r-2a)} \quad (4)$$

where ε is the dielectric constant of the medium (= 80 for water), ε_0 the vacuum permittivity, Ψ_o is the zeta potential and κ^{-1} is the Debye length dependent on the nature of ionic species present and the ionic strength.

$$\kappa = \sqrt{\frac{e^2}{\varepsilon\varepsilon_o KT}\sum_i \varrho_i z_i^2} \quad (5)$$

Where e is the charge of an electron, ϱ_i is the number concentration of ionic species i and z_i is the valence of the ionic species. For 1:1 electrolyte such as NaCl (i=2, z_i = 1), the above equation reduces to

$$\kappa = 3.288\sqrt{I}\,\mathrm{nm}^{-1} \quad (6)$$

Another quantitative measure of the stability of a dispersion against coagulation is expressed by the stability ratio W. The stability ratio is defined as

$$W = \frac{\text{rate of diffusion - controlled aggregation}}{\text{rate of interaction - force controlled aggregation}} \quad (7)$$

The term in the numerator in the above expression is the rate of aggregation in the absence of any interparticle forces or energy barriers and hence is a fast rate of aggregation (purely diffusion). If the value of W is ~ 1 then it implies that there are no force barriers to aggregation and hence the particles are unstable. A high value of W indicates that energy barriers come into play which makes it increasingly difficult for particles to aggregate. An expression for W given a total interaction potential V_T is given below

$$W = 2\int_0^\infty \frac{e^{V_T/kT}}{s^2 G(s)} ds \quad (8)$$

where s = r/a and G(s) is a hydrodynamic factor which takes into account the effect of the suspending medium (solvent) on the motion of the particles.

2.4. Laser Confocal Microscopy

The polarized MDCK cell monolayers were grown using the methods reported in the literature (16). The Transwells® harboring polarized MDCK cell monolayers were transformed into an in-vitro CAA model by pre-incubating them with 25 μg/ml of Aβ protein. Various nanovehicles were added to the pre-incubated monolayers and incubated for 1 hour at 37 °C with gentle shaking. The nanovehicles were removed, the cell surface was washed twice with ice cold HBSS, fixed using 4% paraformaldehyde, mounted, and imaged using Axiovert 100 M microscope equipped with Zeiss LSM 510 laser confocal microscope (excitation = 488 nm; emission = 520 nm, Carl Zeiss, Inc., Thornwood, NY).

3. Results

3.1. Preparation and Characterization of Nanoparticles

a) Chitosan Coated PLGA and PLGA Nanoparticles—Prior to lyophilization, the average particle size of PLGAnp and CPLGAnp was 147.86 ± 18.07 nm and 203.45 ± 5.75 nm, respectively. After lyophilization, the average particle sizes of PLGAnp increased to: 233.57 ± 15.25 nm with 1% mannitol as a cryoprotectant; 174.67 ± 3.12 nm with 1% trehalose; and 206.66 ± 3.52 nm with no cryoprotectant (Figure 2A). In comparison, the particle sizes of CPLGA nanoparticles were significantly lower as they measured 194.55 ± 7.57 nm in the absence of a cryoprotectant, 194.33 ± 6.12 nm and 167.33 ± 2.59 nm in the

presence of 1% mannitol, and 1% trehalose, respectively (Figure 2A). Scanning electron microscope (SEM) images of CPLGAnps showed cubed shaped nanoparticles with an estimated size of 170 nm, in contrast, PLGAnps showed spherical nanoparticles with a large size range of 100–1000nm (Figure 1B–C). The zeta potential of CPLGAnp conjugated with IgG4.1 was 16.80 ± 6.09 mV; CPLGA np, 8.0 ± 1.45 mV; PLGAnp, −4.76 ± 0.74 mV; and PLGAnp conjugated with IgG4.1 was 0.39 ± 0.42 mV- all at pH 7 (Figure 2B).

b) Determining Chitosan Concentration on CPLGA Nanoparticles—Upon interacting with positive charges on the chitosan amine groups, the UV absorbance spectrum of cibacron brilliant red (anionic dye) undergoes a bathochromic shift (Figure 3A) (14). Based on this assay, the amount of chitosan adsorbed on the surface of CPLGA np was determined as 3.09 ± 0.53 μg/mg of nanoparticles (Figure 3D).

c) Preparation and Characterization of 6CMR Loaded PLGAnp and CPLGAnp —The 6CMR was encapsulated in the nanoparticles to visualize the uptake of PLGAnp and CPLGAnp at the cellular barriers. Originally, these nanoparticles were prepared using 1% PVA as the emulsifying agent, which resulted in large particle sizes of 492 ± 7.51 nm (Figure 2C). The particle size of 6CMR-CPLGAnp and 6CMR-PLGAnp reduced with an increase in the PVA concentration and reached plateau values of 217.33 ± 6.82 nm and 267.67 ± 2.52 nm, respectively at 4% PVA concentration (Figure 2C). The zeta potentials of 6CMR-CPLGAnp and 6CMR-PLGAnp were 32.02 ± 2.65 mV and −7.64 mV, respectively at 4% PVA (Figure 2D) and the encapsulation efficiencies were 84.2 ± 4.2 and 83.23 ± 0.66, respectively (Table 1).

The 6CMR-CPLGAnp showed a slight leakage of 6CMR over a period of 48 hrs, which is consistent with other literature reports (17–18), but 6CMR-PLGAnp showed a rapid burst release of 6CMR.

3.2. Preparation and Characterization of Immuno-nanovehicles

a) Conjugation of Anti-Amyloid Antibody (IgG4.1)—when the amount of IgG4.1 in the reaction mixture was increased from 0.2 to 0.5 mg/ml, The IgG4.1 conjugation to the nanocore increased significantly. Further increase in the amount of IgG4.1 to 1.0 mg did not enhance the conjugation (Figure 4A). The extent of IgG4.1 conjugation to control nanovehicles (without chitosan on the surface) was similar to that of immuno-nanovehicles when 0.5 mg IgG4.1 was used in the reaction mixture (Figure 4A).

b) Effect of Lyophilization on Immuno-Nanovehicles—The average particle size of immuno-nanovehicles showed a 25% increase after lyophilization compared to unlyophilized immuno-nanovehicles that showed an average particle size of 265 ± 3.51 nm (Figure 2A). On the other hand, lyophilization of control nanovehicles showed a minimal increase in particle size. A lyophilized physical mixture of PLGAnp/chitosan/IgG4.1 indicated a particle size of 158.7 ± 4.72 nm whereas a lyophilized physical mixture of PLGA/IgG4.1 exhibited a size increase of 207.67 ± 5.28 nm. It should be noted that the same antibody concentration was used in the lyophilized physical mixture as that of the conjugated formulation. The binding of these nanovehicles, before and after lyophilization, to fibrillar Aβ40 was determined by ELISA (Figure 4B). Significantly higher absorbance was observed with immuno-nanovehicles (0.64 ± 0.01) than CPLGAnp conjugated with BSA (0.11 ± 0.01) or unconjugated CPLGAnp (0.18 ± 0.01). On the other hand, control nanovehicles exhibited significantly lower absorbance (0.32 ± 0.01) than the immuno-nanovehicle.

3.3. Stability of Nanovehicle Suspensions

As outlined in the materials and methods section, the colloidal stability of nanovehicles can be predicted based on the total potential energy of interaction (V_T) between two nanovehicles; the larger V_T value corresponds to higher stability. The V_T is a summation of Van Der Waals dispersion forces (V_A) and repulsive forces between the particles (V_E). The VT/kT plot as a function of interparticle separation (r/a) for various nanovehicles developed in this study is presented in Figure 5. As can be seen from this plot and Table 2, the barrier for aggregation ($V_{T\text{-}max}$ or V_T maximum) was the highest for immuno-nanovehicles followed by CPLGAnps and PLGAnps, whereas a maximum in $V_{T\text{-}max}$ /kT value does not exist for control nanovehicles as the attractive Van Der Waals dispersion forces dominate V_T. From the V_T value, the stability ratio (W), which is a direct quantitative measure of the stability of nanovehicles against aggregation, can be calculated. The W of various nanovehicles determined using equations 6 and 7 were presented in Table 1. Like with the $V_{T\text{-}max}$ values, the immuno-nanovehicles showed the highest W followed by CPLGAnps, PLGAnps, and control nanovehicles.

3.4. Uptake of Immuno-Nanovehicles by Polarized MDCK Cell Monolayer

The z-stack images of MDCK cell monolayer treated with 6-coumarin loaded immuno-nanovehicles (6CMR-immuno-nanovehicle) showed substantially greater fluorescence than the monolayers treated with 6-coumarin loaded control nanovehicles (6CMR-control nanovehicle). The x-y image obtained from the center of the z-stack clearly shows cellular internalization of 6CMR-immuno-nanovehicles. Moreover, projections in both x–z and y–z orthogonal planes confirm the transcytosis of 6CMR-immuno-nanovehicles across the MDCK cell monolayer (Figure 6A). However, much lower fluorescence intensity was observed in the MDCK cell monolayer treated with 6CMR-control nanovehicle (Figure 6B). Both images were obtained using the same microscope settings. Furthermore, the x-z images of the monolayers treated with 6CMR-immuno-nanovehicle (Figure 6D) showed higher fluorescence than those treated with 6CMR-CPLGAnp (Figure 6C). More interestingly, the 6CMR-immuno-nanovehicle uptake increased substantially in the MDCK cell monolayers treated with Aβ proteins (Figure 6E).

4. DISCUSSION

Polymers adsorbed on the surface of nanoparticles were shown to modify their aggregation propensity, sedimentation properties, and rheological behavior. In addition, the adsorbed polymers were claimed to improve the interactions of the nanoparticles with biological systems, which may result in enhanced uptake at cellular barriers and increased residence time in the body (19–20). In the current study, we have demonstrated that the surface adsorption of chitosan, a polycationic polymer, improves the stability of nanoparticles during lyophilization; lowers their propensity to aggregate in aqueous solutions; protects the antibodies conjugated to the nanoparticle surface; and enhances their cellular uptake. By imparting these critical attributes, chitosan greatly simplifies the design of immuno-nanovehicles intended for the treatment and diagnosis of AD and CAA.

Adsorption of chitosan on the surface of PLGAnp have been attempted previously. Guo and Gemeinhart (21) have demonstrated that chitosan follows Langmuir model of monolayer adsorption at lower concentrations (<0.5 g/L), but at higher chitosan concentrations it shifts to multilayer adsorption. Moreover, when used with low concentrations of the stabilizer (0.5% PVA), higher chitosan concentrations in the aqueous phase increased the nanoparticle size to approximately 900 nm. In case of immuno-nanovehicles intended for targeting cerebrovascular amyloid, a complete coverage of the surface by chitosan interfered with the conjugation of polyamine modified anti-amyloid antibody (IgG4.1) to the nanovehicles (data

not shown). Moreover, an increase in the nanoparticle size due to higher chitosan adsorption may restrict their ability to cross the BBB (Figure 2A). Therefore, the size of CPLGAnp was controlled by regulating the amount of chitosan in aqueous phase and by increasing PVA concentration in the formulation (Figure 2A, 2C). While increases in the PVA concentration did not affect the size of 6CMR-PLGAnp, the 6CMR-CPLGAnp size decreased with an increase in the PVA concentration and reached a plateau at 4% concentration (Figure 2C). As expected, the 6CMR-PLGAnp exhibited a negative zeta potential (<−8 mV) whereas the 6CMR-CPLGAnp exhibited a positive zeta potential above 20 mV (Figure 2D).

The IgG4.1 was conjugated to the surface of control or immuno-nanovehicles through carbodiimide conjugation, which covalently links an amine group to a carboxylic group. Although IgG4.1 could be linked to the amine groups on the chitosan or the carboxylic groups on the nanocore, it was determined that the optimal conjugation is achieved by targeting the carboxylic groups on the nanocore (data not shown). The IgG4.1 conjugation to the immuno-nanovehicle increased linearly with an increase in IgG4.1 concentration in the reaction mixture and saturated at 0.5 mg/ml IgG4.1 concentration, most likely due to the unavailability of free carboxylic groups on the nanocore due to adsorbed chitosan (Figure 4A).

The stability of various nanovehicles under low salt concentrations was assessed based on the DLVO theory. At any temperature T, a particle possesses an average thermal energy of 1 kT. If the maximum in V_T (barrier for aggregation) is higher than the average thermal energy of 1kT then the particles become colloidally stable. It is evident from the data presented in Figure 6 and Table 1 that the barrier for aggregation increased 2.85 times due to the presence of chitosan on CPLGAnp. In addition, conjugating IgG4.1 to the surface of CPLGAnp increased the $V_{T\text{-}max}/kT$ value from 4.92 to 37.8. This energy barrier is too steep for the immuno-nanovehicles thus formed to overcome and aggregate, hence they are colloidally stable. On the other hand, conjugating IgG4.1 to PLGAnp worsens the stability. The PLGAnp have a negative charge on their surface that gives rise to a barrier of 1.73 kT. Conjugating positively charged IgG4.1 reduces the magnitude of repulsion between the control nanovehicles and a $V_{T\text{-}max}$ no longer exists; hence they are colloidally unstable. The stability ratios (W) of various nanovehicles provided in Table 1 also point out that immuno-nanovehicles are the most stable against aggregation followed by CPLGAnp and PLGAnp. Addition of chitosan to PLGAnps increased their W by 16 fold and the conjugation of IgG4.1 to form immuno-nanovehicles further enhanced the W values at least by 10^{15} fold. However, IgG4.1 in the absence of chitosan was unable to show such an effect, which can be inferred from the large differences in the W values of immuno-nanovehicles and control nanovehicles.

Lyophilization increases the shelf life of a nanovehicle formulation. However, in the absence of a cryoprotectant, lyophilization could denature the antibodies conjugated to the nanovehicle surface, cause nanovehicles to aggregate, and trigger the leakage of the entrapped drug (22–23). Cryoprotectants such as trehalose, mannitol, and sucrose are added to the formulation to prevent such undesirable changes during lyophilization. Although, sugars are widely used as cryoprotectants, polymers such as dextran have shown the ability to protect nanovehicles during lyophilization. Dextran adsorbs to the surface of nanoparticles and shields them from mechanical stress generated during the lyophilization (22, 24). Studies have indicated that low molecular weight chitosan nanoparticles (25) and poly(epsilon-caprolactone) nanocapsules (23) formulated at higher PVA concentrations required no cryoprotectant, thereby, suggesting that chitosan and PVA act as cryoprotectants in these cases. The chitosan's ability to function as a cryoprotectant comes from D-glucosamine groups that structurally resemble sugars (26).

In the current study, we studied the efficacy of chitosan to prevent aggregation, leakage of encapsulated 6-CMR from PLGA nanocore, and denaturation of IgG4.1 during lyophilization. The particle sizes of both 6CMR-immuno-nanovehicles and 6CMR-control nanovehicles slightly increased after lyophilization. However, lyophilization of PLGA-6CMRnp resulted in a burst release of encapsulated 6-CMR, which is indicative of compromised nanocore, but the leakage of 6-CMR from 6CMR-CPLGAnp was very limited (17). Furthermore, immuno-nanovehicles, lyophilized or unlyophilized were able to bind to Aβ, but not lyophilized or unlyophilized control nanovehicles. In addition, a physical mixture of chitosan, PLGA and IgG4.1 recognized Aβ40 but not the physical mixture of PLGA and IgG4.1 (Figure 4B). The role of chitosan in preserving IgG4.1 was verified when IgG4.1 lyophilized with chitosan bound to Aβ40 twice as much as that lyophilized without chitosan (Figure 4B). These results indicate that chitosan effectively preserves the integrity nanocore and IgG4.1 conjugated to the surface of immuno-nanovehicles.

Chitosan is endowed with positive charges from the protonated amines that help nanovehicles to anchor to the negatively charged cell surface. Such electrostatic interaction with the cell surface was shown to enhance the cellular uptake of many cationic proteins and even nanovehicles. Therefore, the positive charge density on the nanovehicles imparted by chitosan is not only critical for maintaining their colloidal stability but also play a vital role in enhancing their cellular uptake. The pK_a of amine groups on chitosan is around 6.2 (27–28). Consequently, the zeta potential of CPLGA nanoparticles is as high as 20 mV at pH 5 and drops to 10 mV at physiological pH. However, the zeta potential restored to 16.80 mV when IgG4.1 was conjugated to the nanovehicles most likely due to the involvement of carboxyl groups in the carbodiimide reaction such that the protonated amines on the adsorbed chitosan are exposed. On the other hand, the engagement of carboxyl groups on the control nanovehicles during IgG4.1 conjugation brings the zeta potential value of the nanovehicles closer to zero (Figure 2B), which impacts their colloidal stability and reduces their cellular uptake. Furthermore, chitosan promotes the formation of a cube or rod shaped particles (Figure 1), which was shown to have a better cellular penetration than a spherical particle (5, 27).

The laser confocal images of polarized MDCK cells monolayer, a commonly used in vitro BBB model, treated with immuno-nanovehicles clearly showed that they were transcytosed across the monolayer and also moved through the pores of the filter support, which appears as columns of bright fluorescence (Figure 6). But, the transcytosis was not evident with control nanovehicles; only faint intracellular fluorescence was seen. These results clearly demonstrate that the surface adsorbed chitosan promotes the transcytosis of immuno-nanovehicles across the BBB in vitro. In addition, a significant increase in the uptake of 6CMR-immuno-nanovehicles was observed in the cells treated with Aβ40 antigen (Figure 6E). This demonstrates the ability of these immuno-nanovehicles to selectively target the intracellular Aβ40 antigen.

In this study, we have successfully designed a prototype immuno-nanovehicle that is capable of targeting cerebrovascular amyloid proteins. The nanoparticle size is maintained around 200 nm, so that they are retained in the cerebral vasculature and not diffuse into brain parenchyma. Chitosan adsorbed on the surface of nanovehicles prevented their aggregation in aqueous suspensions and greatly enhanced their colloidal stability as determined based on DLVO theory. Furthermore, chitosan imparted cryoprotection to the nanocore and also to the conjugated IgG4.1. More importantly, chitosan enhanced the transcytosis of nanovehicles across the BBB model in vitro. In addition, the immuno-nanovehicles showed the ability to selectively target intracellular Aβ antigen, and thereby demonstrated their potential as diagnostic and therapeutic nanovehicles to detect and treat CAA and AD.

Acknowledgments

The authors acknowledge the financial assistance provided by Alzheimer's Association grant NIRG-09-133017 (KKK); NIH/NCRR/RCMI grant G12RR03020 (KKK): Neuroscience Cores for MR Studies of the Brain from NINDS grant number NS 057091 (JFP), and the Minnesota Partnership for Biotechnology and Medical Genomics (JFP). The sponsor had no role in study design, collection, data analysis, data interpretation, and played no role in the decision to submit this paper for publication.

Abbreviations

CVA	cerebrovascular amyloid
CAA	cerebral amyloid angiopathy
BBB	blood brain barrier
PLGA	poly lactic-co-glycolic acid
PLGAnp	PLGA nanoparticles
CPLGAnp	chitosan coated PLGA nanoparticles
6CMR	6-Coumarin
IgG4.1	anti-amyloid antibody 4.1
EDAC	n-(3-dimethylaminopropyl)-n'-ethylcarbodiimide hydrochloride
NHS	n-hydroxysuccinimide
PBS	phosphate buffered saline
PVA	poly vinyl alcohol
BSA	bovine serum albumin
DCM	dichloromethane
6CMR	6-Coumarin
MDCK	Madin-Darby Canine Kidney
DMEM	Dulbecco's modified eagle's medium
FBS	fetal bovine serum
SEM	scanning electron microscope
ELISA	Enzyme Linked Immunosorbent Assay
Aβ	Amyloid Beta protein

References

1. Calhoun ME, Burgermeister P, Phinney AL, Stalder M, Tolnay M, Wiederhold KH, Abramowski D, Sturchler-Pierrat C, Sommer B, Staufenbiel M, Jucker M. Neuronal overexpression of mutant amyloid precursor protein results in prominent deposition of cerebrovascular amyloid. Proc Natl Acad Sci U S A. 1999 Nov 23;96(24):14088–14093. [PubMed: 10570203]
2. Ulbrich K, Hekmatara T, Herbert E, Kreuter J. Transferrin- and transferrinreceptor-antibody-modified nanoparticles enable drug delivery across the blood-brain barrier (BBB). Eur J Pharm Biopharm. 2009 Feb; 71(2):251–256. [PubMed: 18805484]
3. Chang J, Jallouli Y, Kroubi M, Yuan XB, Feng W, Kang CS, Pu PY, Betbeder D. Characterization of endocytosis of transferrin-coated PLGA nanoparticles by the blood-brain barrier. Int J Pharm. 2009 Sep 11;379(2):285–292. [PubMed: 19416749]
4. Agyare EK, Curran GL, Ramakrishnan M, Yu CC, Poduslo JF, Kandimalla KK. Development of a smart nano-vehicle to target cerebrovascular amyloid deposits and brain parenchymal plaques

observed in Alzheimer's disease and cerebral amyloid angiopathy. Pharm Res. 2008 Nov; 25(11): 2674–2684. [PubMed: 18712585]

5. Muro S, Garnacho C, Champion JA, Leferovich J, Gajewski C, Schuchman EH, Mitragotri S, Muzykantov VR. Control of endothelial targeting and intracellular delivery of therapeutic enzymes by modulating the size and shape of ICAM-1-targeted carriers. Mol Ther. 2008 Aug; 16(8):1450–1458. [PubMed: 18560419]
6. Rensen PC, de Vrueh RL, Kuiper J, Bijsterbosch MK, Biessen EA, van Berkel TJ. Recombinant lipoproteins: lipoprotein-like lipid particles for drug targeting. Adv Drug Deliv Rev. 2001 Apr 25; 47(2–3):251–276. [PubMed: 11311995]
7. Poduslo JF, Ramakrishnan M, Holasek SS, Ramirez-Alvarado M, Kandimalla KK, Gilles EJ, Curran GL, Wengenack TM. In vivo targeting of antibody fragments to the nervous system for Alzheimer's disease immunotherapy and molecular imaging of amyloid plaques. J Neurochem. 2007 Jul; 102(2): 420–433. [PubMed: 17596213]
8. Banks WA, Akerstrom V, Kastin AJ. Adsorptive endocytosis mediates the passage of HIV-1 across the blood-brain barrier: evidence for a post-internalization coreceptor. J Cell Sci. 1998 Feb; 111(Pt 4):533–540. [PubMed: 9443901]
9. Kandimalla KK, Wengenack TM, Curran GL, Gilles EJ, Poduslo JF. Pharmacokinetics and amyloid plaque targeting ability of a novel peptide-based magnetic resonance contrast agent in wild-type and Alzheimer's disease transgenic mice. J Pharmacol Exp Ther. 2007 Aug; 322(2):541–549. [PubMed: 17505020]
10. Ramakrishnan M, Kandimalla KK, Wengenack TM, Howell KG, Poduslo JF. Surface plasmon resonance binding kinetics of Alzheimer's disease amyloid beta peptide-capturing and plaque-binding monoclonal antibodies. Biochemistry. 2009 Nov 3;48(43):10405–10415. [PubMed: 19775170]
11. Ramakrishnan M, Wengenack TM, Kandimalla KK, Curran GL, Gilles EJ, Ramirez-Alvarado M, Lin J, Garwood M, Jack CR Jr. Poduslo JF. Selective contrast enhancement of individual Alzheimer's disease amyloid plaques using a polyamine and Gd-DOTA conjugated antibody fragment against fibrillar Abeta42 for magnetic resonance molecular imaging. Pharm Res. 2008 Aug; 25(8):1861–1872. [PubMed: 18443900]
12. Yang R, Shim WS, Cui FD, Cheng G, Han X, Jin QR, Kim DD, Chung SJ, Shim CK. Enhanced electrostatic interaction between chitosan-modified PLGA nanoparticle and tumor. Int J Pharm. 2009 Apr 17; 371(1–2):142–147. [PubMed: 19118614]
13. Yang R, Yang SG, Shim WS, Cui F, Cheng G, Kim IW, Kim DD, Chung SJ, Shim CK. Lung-specific delivery of paclitaxel by chitosan-modified PLGA nanoparticles via transient formation of microaggregates. J Pharm Sci. 2009 Mar; 98(3):970–984. [PubMed: 18661542]
14. Muzzarelli RA. Colorimetric determination of chitosan. Anal Biochem. 1998 Jul 1; 260(2):255–257. [PubMed: 9657888]
15. Wischke C, Borchert HH. Increased sensitivity of chitosan determination by a dye binding method. Carbohydr Res. 2006 Dec 29; 341(18):2978–2979. [PubMed: 17087922]
16. Irvine JD, Takahashi L, Lockhart K, Cheong J, Tolan JW, Selick HE, Grove JR. MDCK (Madin-Darby canine kidney) cells: A tool for membrane permeability screening. J Pharm Sci. 1999 Jan; 88(1):28–33. [PubMed: 9874698]
17. Corrigan OI, Li X. Quantifying drug release from PLGA nanoparticulates. Eur J Pharm Sci. 2009 Jun 28; 37(3–4):477–485. [PubMed: 19379812]
18. Qaddoumi MG, Ueda H, Yang J, Davda J, Labhasetwar V, Lee VH. The characteristics and mechanisms of uptake of PLGA nanoparticles in rabbit conjunctival epithelial cell layers. Pharm Res. 2004 Apr; 21(4):641–648. [PubMed: 15139521]
19. Zhao J, Liu CS, Yuan Y, Tao XY, Shan XQ, Sheng Y, Wu F. Preparation of hemoglobin-loaded nano-sized particles with porous structure as oxygen carriers. Biomaterials. 2007 Mar; 28(7): 1414–1422. [PubMed: 17126898]
20. Sheng Y, Liu C, Yuan Y, Tao X, Yang F, Shan X, Zhou H, Xu F. Long-circulating polymeric nanoparticles bearing a combinatorial coating of PEG and water-soluble chitosan. Biomaterials. 2009 Apr; 30(12):2340–2348. [PubMed: 19150737]

21. Guo C, Gemeinhart RA. Understanding the adsorption mechanism of chitosan onto poly(lactide-co-glycolide) particles. Eur J Pharm Biopharm. 2008 Oct; 70(2):597–604. [PubMed: 18602994]

22. Abdelwahed W, Degobert G, Stainmesse S, Fessi H. Freeze-drying of nanoparticles: formulation, process and storage considerations. Adv Drug Deliv Rev. 2006 Dec 30; 58(15):1688–1713. [PubMed: 17118485]

23. Abdelwahed W, Degobert G, Fessi H. A pilot study of freeze drying of poly(epsilon-caprolactone) nanocapsules stabilized by poly(vinyl alcohol): formulation and process optimization. Int J Pharm. 2006 Feb 17; 309(1–2):178–188. [PubMed: 16326053]

24. Aumelas A, Serrero A, Durand A, Dellacherie E, Leonard M. Nanoparticles of hydrophobically modified dextrans as potential drug carrier systems. Colloids Surf B Biointerfaces. 2007 Sep 1; 59(1):74–80. [PubMed: 17560095]

25. Kim DG, Jeong YI, Choi C, Roh SH, Kang SK, Jang MK, Nah JW. Retinolencapsulated low molecular water-soluble chitosan nanoparticles. Int J Pharm. 2006 Aug 17; 319(1–2):130–138. [PubMed: 16713152]

26. Pillai CKS, Paul W, Sharma CP. Chitin and chitosan polymers: Chemistry, solubility and fiber formation. Progress in Polymer Science. 2009; 34(7):641–678.

27. Zhang K, Rossin R, Hagooly A, Chen Z, Welch MJ, Wooley KL. Folate-mediated Cell Uptake of Shell-crosslinked Spheres and Cylinders. J Polym Sci A Polym Chem. 2008; 46(22):7578–7583. [PubMed: 19855851]

28. Russel, WB.; Saville, DA.; Schowalter, WR. Colloidal Dispersions. Cambridge University Press; 1992.

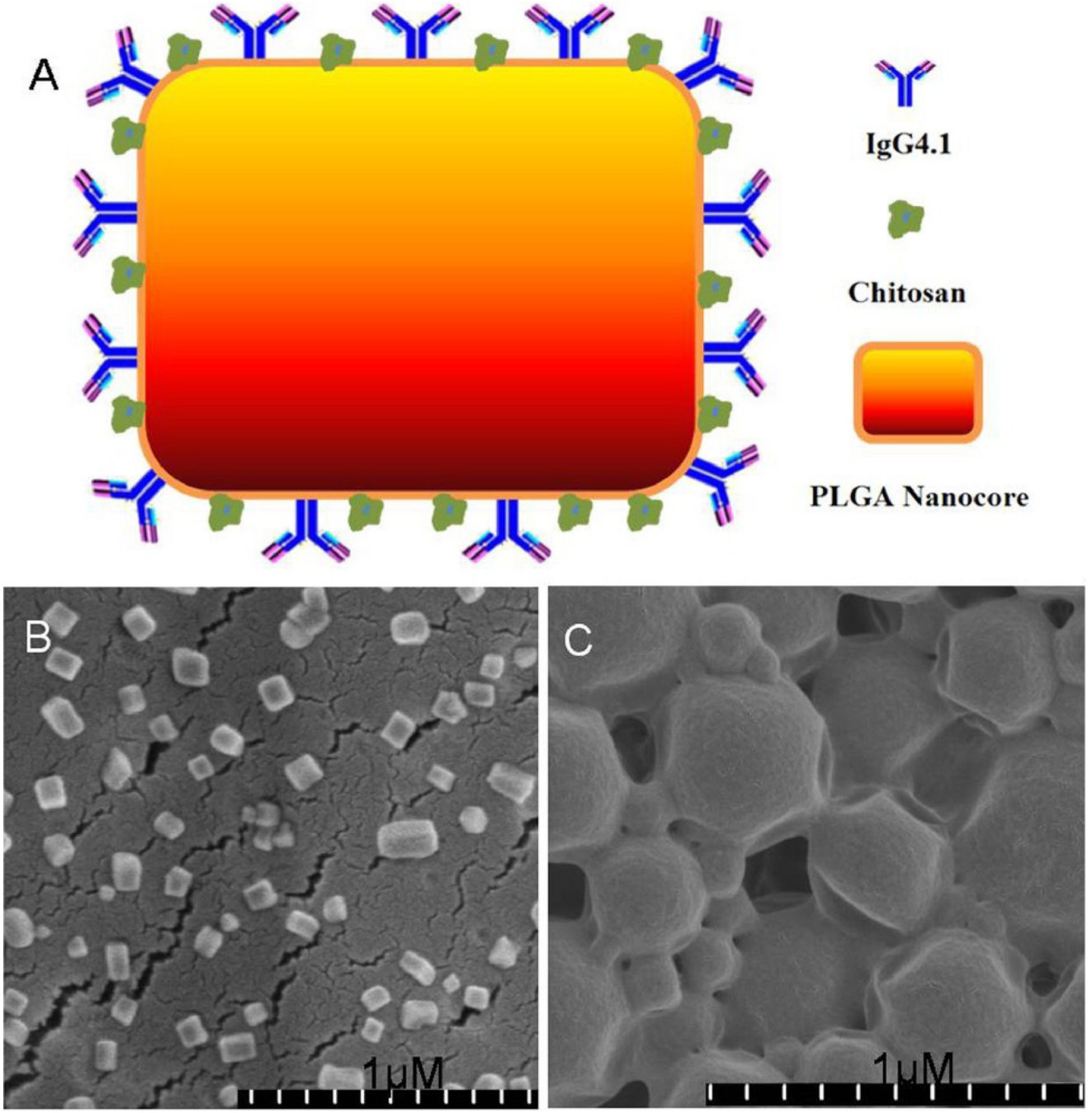

Figure 1.

A. A schematic representation of chitosan coated PLGA nanovehicles with surface IgG4.1 antibody conjugated on the surface.

B. Scanning electron micrograph (SEM) of chitosan coated PLGA nanovehicles.

C. SEM micrograph of PLGA nanovehicles.

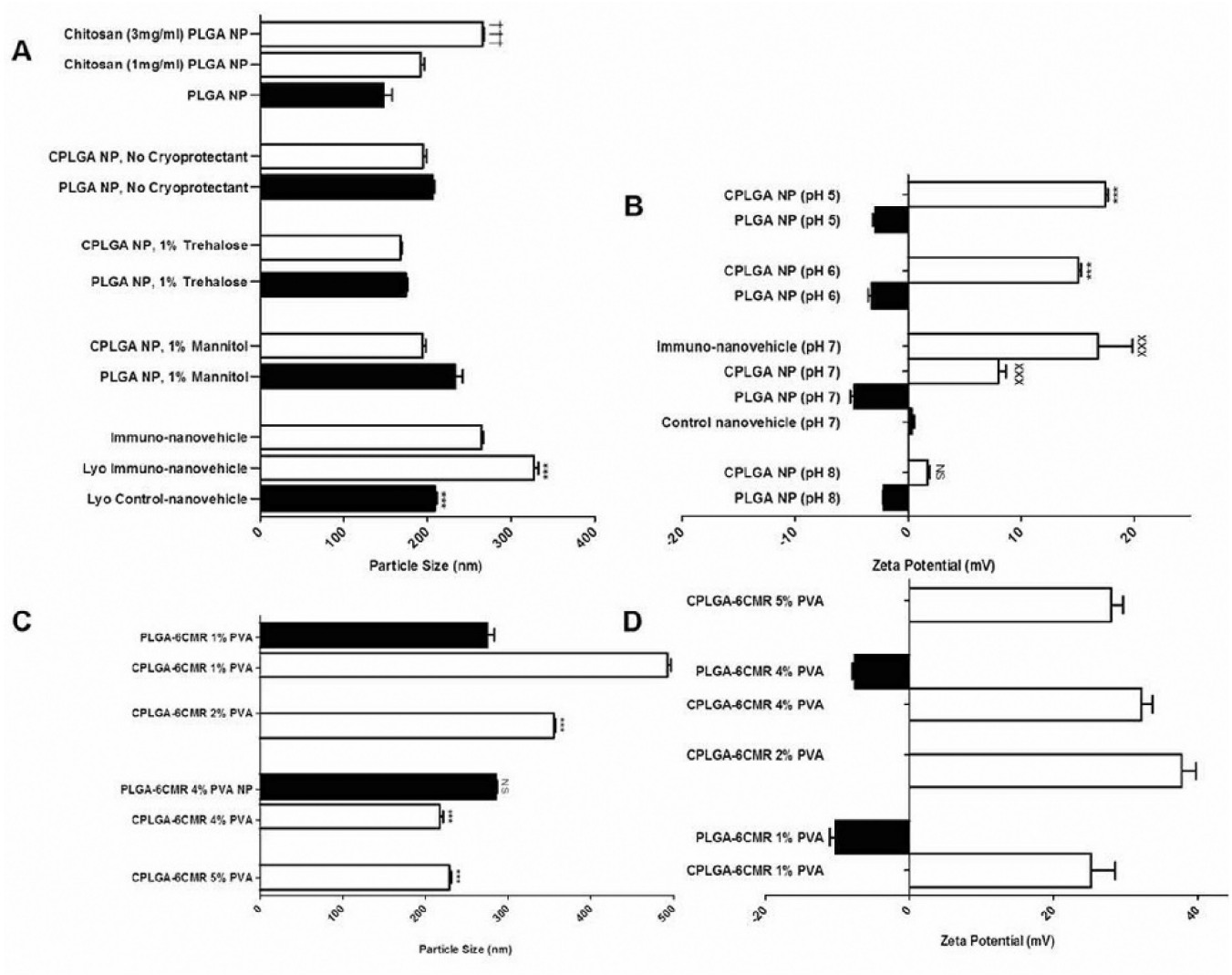

Figure 2.

A. Average particle size of nanovehicles measured under various formulation and lyophilization conditions. Comparisons among mean particle sizes were made using one-way Anova followed by Tukey post-test. $^{\dagger\dagger\dagger}p<0.001$ (n = 3): Chitosan (3 mg/ml) coated PLGAnp versus chitosan (1 mg/ml) PLGAnp or PLGAnp. ***$p<0.001$ (n = 3): lyophilized PLGA nanovehicles conjugated with IgG4.1 (control nanovehicles) or lyophilized Chitosan coated PLGA nanovehicles conjugated with IgG4.1 (immuno-nanovehicles) (both lyophilized with 1% trehalose and 0.02% tween) versus unlyophilized immuno-nanovehicles.

B. Effect of pH on the average zeta potential of chitosan coated PLGA (CPLGA) and PLGA (without chitosan) nanovehicles with and without IgG4.1. All of these nanoparticles were prepared using 4% PVA concentration. Comparisons among zeta potential values were made using one-way Anova followed by Tukey post-test. ***$p<0.001$ (n = 3): CPLGAnp versus PLGAnp at pH values 5 and 6. $^{xxx}p<0.001$ (n = 3): CPLGAnp or immuno-nanovehicles (CPLGA-IgG4.1) versus control nanovehicles (PLGA-IgG4.1) and PLGAnp at pH 7. N.S: PLGAnp versus CPLGAnp at pH 8.

C. Effect of PVA content on the average particle size of 6-coumarin loaded chitosan coated PLGA (6CMR-CPLGAnp) and 6-coumarin loaded PLGA (6CMR-PLGAnp) nanoparticles. Comparisons among mean particle size were made using oneway Anova followed by Tukey post-test. ***$p<0.001$ ($n = 3$): 6CMR-CPLGAnp prepared with 1% PVA versus 6CMR-CPLGAnp prepared with PVA concentrations of 2%, 4%, or 5%; N.S: 6CMR-PLGAnp prepared with 1% PVA versus 6CMR-PLGAnp prepared with 4% PVA.
D. The effect of PVA content on the average zeta potential of 6CMR-CPLGA and 6CMR-PLGAnp.

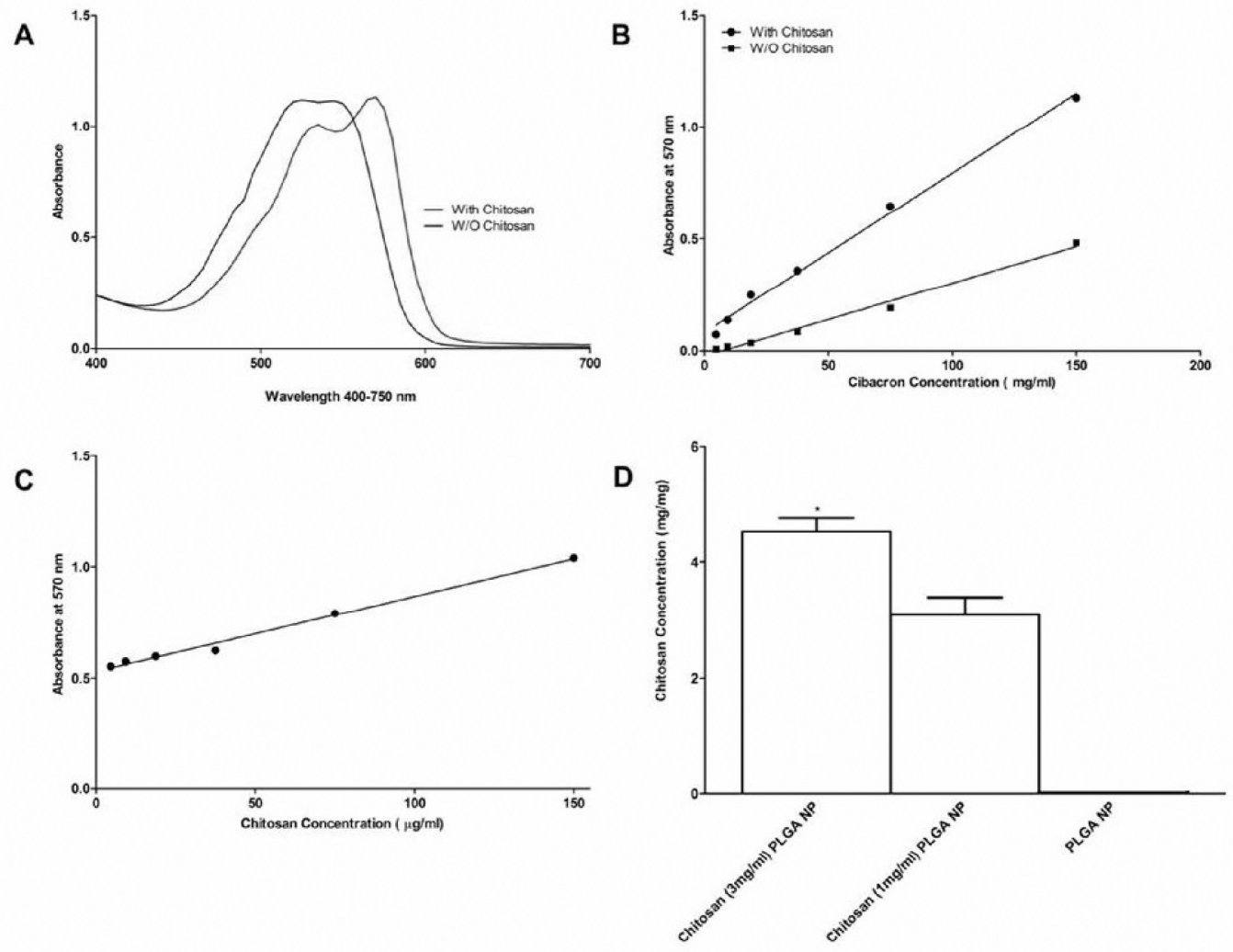

Figure 3.

A. A spectrum of cibacron red in the presence of chitosan clearly shows a bathochromic shift from that obtained in the absence of chitosan.

B. Standard Curves for Cibacron Red with 250 µg/ml chitosan and without chitosan.

C. Chitosan Standard Curve with 150 µg/ml Cibacron red.

D.The amount of chitosan was determined by measuring the differences in the absorbance of cibacron red in the presence of PLGA nanoparticles with and without chitosan. Comparisons among mean chitosan concentrations were made using oneway Anova followed by Tukey post-test. *$p<0.05$ ($n = 3$): chitosan coated PLGA nanoparticles (CPLGAnp) versus uncoated PLGA nanoparticles (PLGAnp).

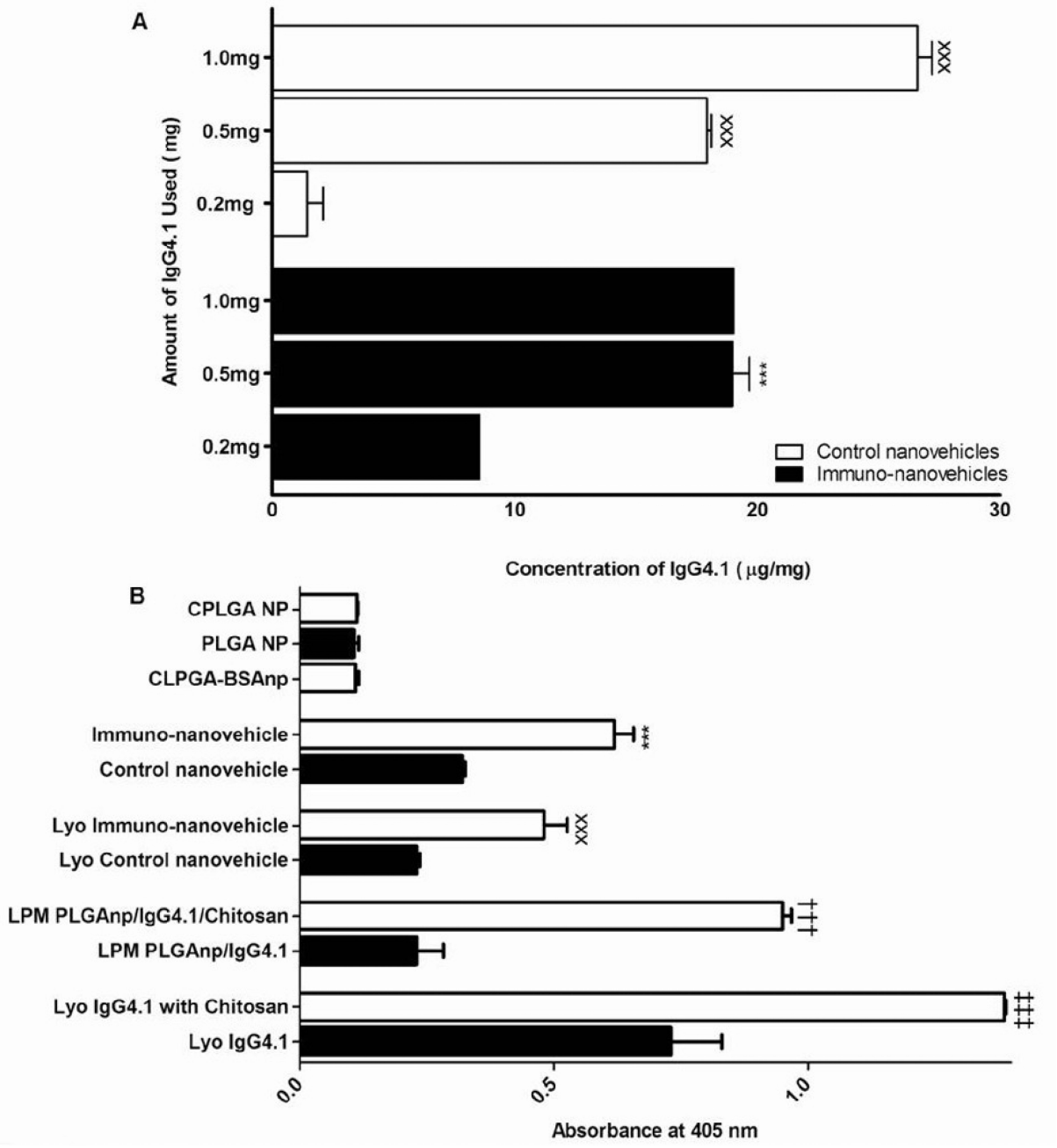

Figure 4.

A. The effect of IgG4.1 concentration in the reaction mixture on the amount of IgG4.1 conjugated to the nanovehicle surface at pH 7. Comparisons among means were made using one-way Anova followed by Tukey post-test. ***$p<0.001$ ($n = 3$): chitosan coated PLGA nanovehicles (CPLGA-IgG4.1 immuno-nanovehicles) conjugated with 0.5 mg of IgG4.1 versus 0.2 mg; $^{xxx}p<0.001$ ($n = 3$) PLGA nanovehicles (PLGA-IgG4.1 immuno-nanovehicles) conjugated with 1.0 mg and 0.5 mg PLGA-IgG4.1 immuno-nanovehicles versus 0.2 mg PLGA-IgG4.1 immuno-nanovehicles.

B. The binding of various nanovehicle formulations to fibrillar Aβ40. Comparisons among mean absorbance were made using one-way Anova followed by Tukey post-test. ***p<0.001 (n = 9): chitosan coated PLGA nanovehicles conjugated with IgG4.1 (immuno-nanovehicles) versus PLGA nanovehicles conjugated with IgG4.1 (control nanovehicles); ^{xxx}p<0.001 (n = 9): lyophilized immuno-nanovehicles versus lyophilized control nanovehicles; †††p<0.001 (n = 9): lyophilized physical mixture (LPM) of PLGAnp/Chitosan/IgG4.1 versus LPM of PLGAnp/IgG4.1; ***p<0.001 (n = 9): LPM of IgG4.1/Chitosan versus IgG4.1. All lyophilized formulations containing IgG4.1 were lyophilized with 1% trehalose and 0.02% tween 20.

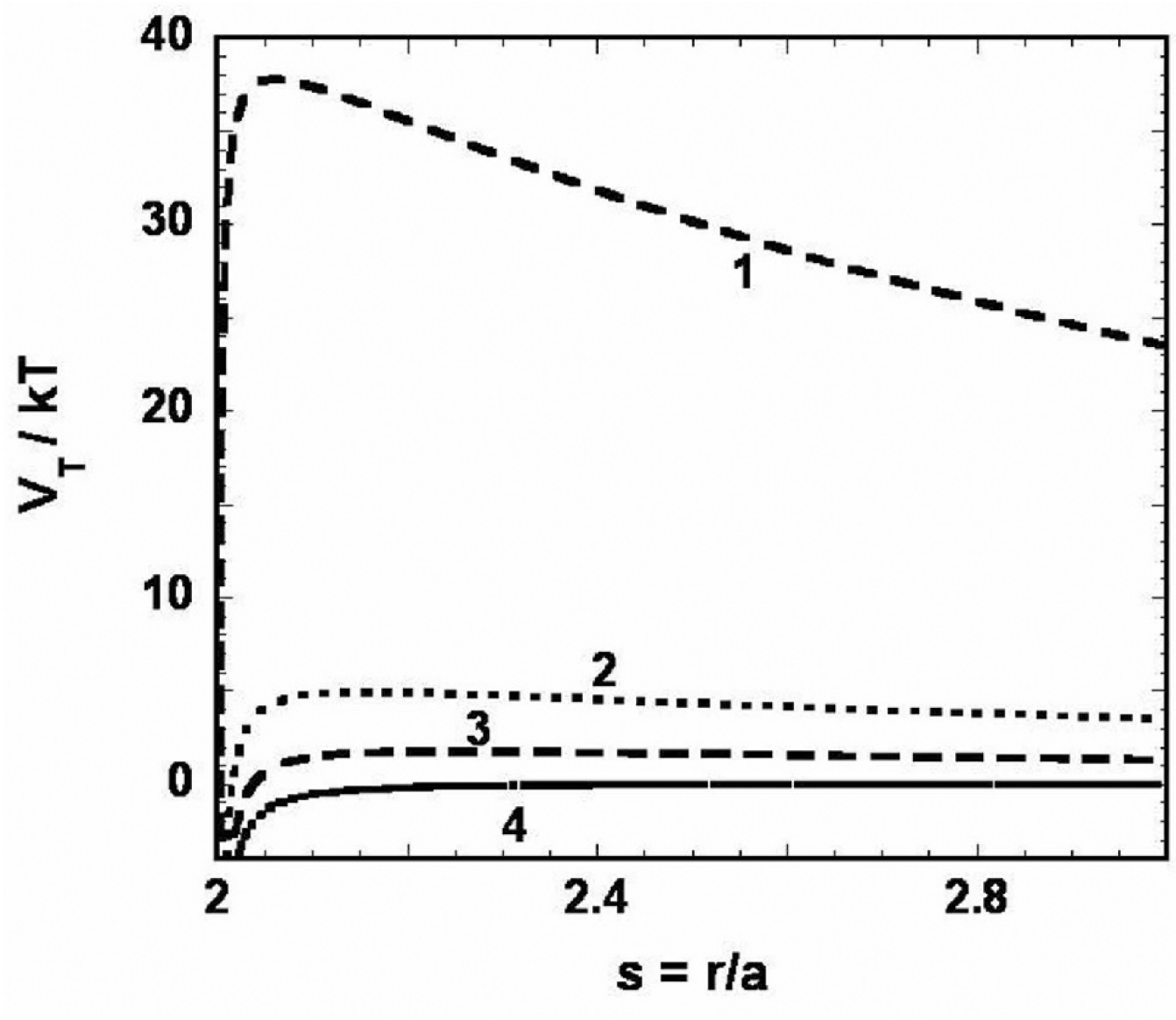

Figure 5.

Total interaction energy (V_T/kT – calculated using equations 1–3) as a function of interparticle separation (r/a) for the different nanovehicles used in this work - CPLGA-IgG4.1 immuno-nanovehicles (1), CPLGAnp (2), PLGA-IgG4.1 control nanovehicles (3), and PLGAnp (4). Values of the parameters used in the calculation of V_T are given in table 1. A hamaker constant of 0.5×10^{-20} J was used for all the nanoparticles.

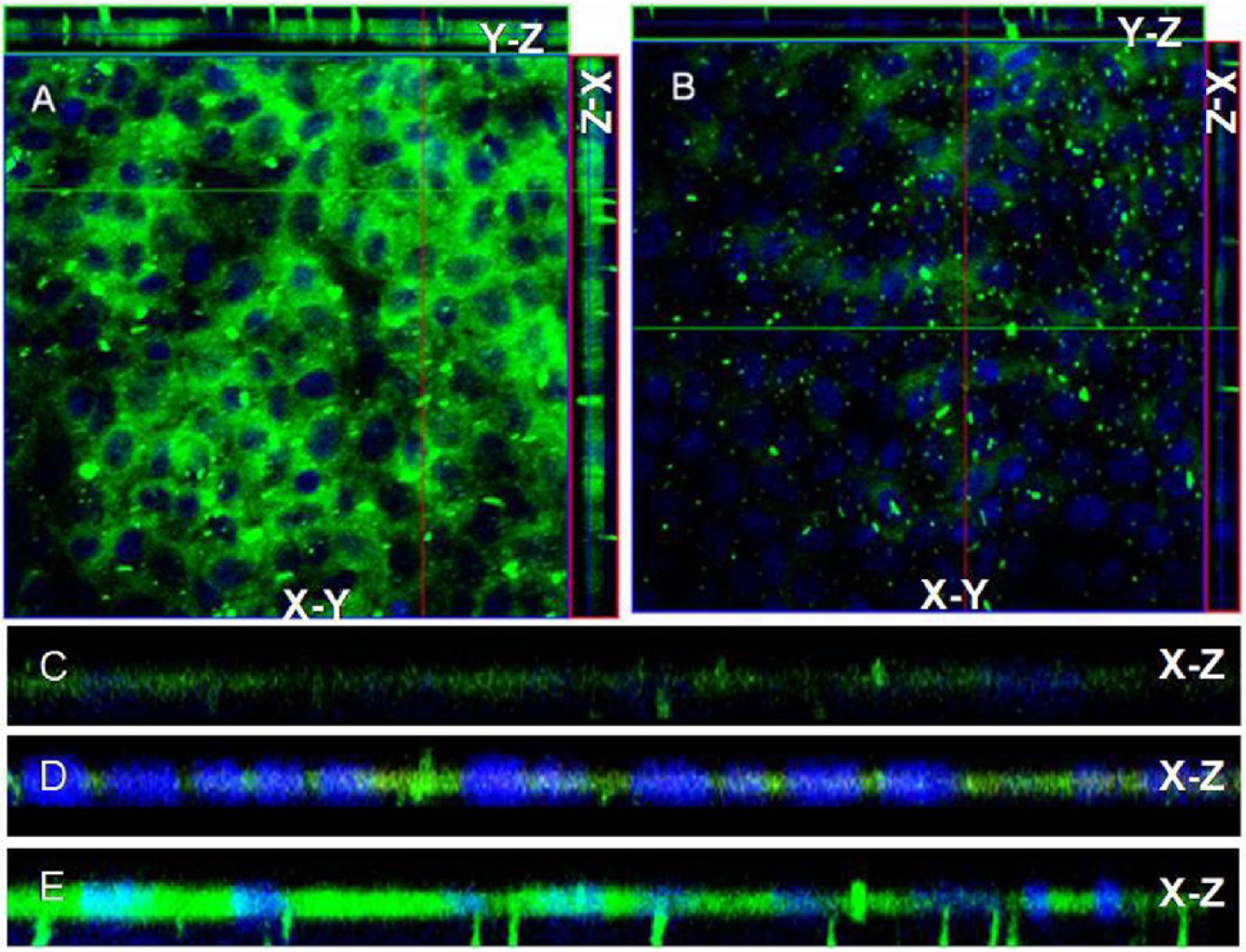

Figure 6.

Uptake of (A) 6-coumarin loaded chitosan coated PLGA nanovehicles conjugated with IgG4.1 (immuno-nanovehicles); (B) 6-coumarin loaded PLGA nanovehicles conjugated with IgG4.1 (control nanovehicles); (C) 6-coumarin chitosan coated PLGAnp (6CMR-CPLGAnp); (D)immuno-nanovehicles; in MDCK cells and (E) immuno-nanovehicles in MDCK cells challenged with $A\beta_{40}$ determined by laser confocal microscopy. All z-stack images were obtained under the same microscope settings and the X-Y plane images presented was obtained from the center of the Z-stack.

Table 1

The encapsulation efficiency of chitosan coated PLGA (CPLGA) and PLGA nanoparticles unlyophilized (UL) and lyophilized with no cryoprotectant (NC) or 1% trehalose.

Type of Nanoparticle	Encapsulation Efficiency (%)
CPLGA-UL	84.24 ± 4.22
CPLGA-NC	91.15 ± 0.49
PLGA-1% Trehalose	83.23 ± 0.66

Table 2

Parameters that impact the colloidal stability of various nanovehicles developed in this study.

#	Nanovehicle Type	Particle Diameter 2a (nm)	Zeta Potential Ψ_o (mV)	Potential Energy Maximum $V_{T\text{-}max}/kT$	Stability Ratio W
1	Immuno-nanovehicle	265	16.8	37.8	7.08×10^{15}
2	CPLGA	165	8.0	4.92	109.4
3	PLGA	174	−4.76	1.73	6.83
4	Control nanovehicle	175	0.39	N/A	1.79